EARTHQUAKE ENGINEERING AND STRUCTURAL DYNAMICS
Earthquake Engng. Struct. Dyn. **28**, 255–272 (1999)

APPLICATION OF WAVELETS TO ANALYSIS AND SIMULATION OF EARTHQUAKE MOTIONS

JUN IYAMA† AND HITOSHI KUWAMURA*,‡

Engineering Research Institute, School of Engineering, The University of Tokyo, 2-11-16 Yayoi, Bunkyo-ku, Tokyo, 113-8656, Japan

SUMMARY

A method of applying wavelet transform to earthquake motion analysis is developed from the viewpoint of energy input structures, in which relationships between wavelet coefficients and energy input, namely energy principles in wavelet analysis are derived. By using the principles, time–frequency characteristics of the 1995 Hyogoken-Nanbu earthquake ground motions are analysed and time histories of energy input for various ranges of frequencies and epicentral distances are identified. Furthermore, a technique to simulate earthquake ground accelerations by wavelet inverse transform is developed on the condition that target time-frequency characteristics are specified. Structural responses to the simulated accelerations are compared with the target time–frequency characteristics, which shows satisfactory correlations between wavelet coefficients and energy responses in both time and frequency domains. Copyright © 1999 John Wiley & Sons, Ltd.

KEY WORDS: wavelet transform; simulated earthquake motions; energy input; Fourier transform; time–frequency characteristics; energy input rate

1. INTRODUCTION

Energy introduced to a structure by an earthquake has been considered an important factor related to structural damage.[1–7] Especially, energy input from the beginning to the end of earthquake motions, which is called total energy input, is useful in design procedures, because the spectrum of energy-based equivalent velocity with respect to natural period is basically same as the Fourier amplitude spectrum obtained from ground accelerations with a supplementary application of smoothing techniques.[8] This supports the empirical observation that the energy-based equivalent velocity is affected primarily by the natural period of a structure but scarcely by other factors such as yield strength and hysteresis shape, and thus the design criterion that energy absorption capacity of a structure should be greater than the total energy input was easily established for survival of the structure against a severe earthquake.[4] Furthermore, earthquake load effect in terms of energy input for probability-based design was defined to be statistically independent of structural resistance, which enabled the application of Load and Resistance Factor Design (LRFD) approach to seismic design in the same way as to gravity design.[5]

* Correspondence to: Hitoshi Kuwamura, Engineering Research Institute, School of Engineering, The University of Tokyo, 2-11-16 Yayoi, Bunkyo-ku, Tokyo, 113-8656, Japan. E-mail: kuwamura@stahl.arch.t.u-tokyo.ac.jp
† Research Associate
‡ Associate Professor

CCC 0098–8847/99/030255–18$17·50

Received 26 February 1998
Revised 25 August 1998

However, dynamic behaviours of inelastic structures during an earthquake are very complex non-stationary processes which are affected by random characteristics of earthquake motions not only in the frequency domain but also in the time domain. Therefore, structural safety in earthquake dynamics cannot be estimated by the above-mentioned energy spectra defined only in the frequency domain. For example, the Hachinohe motions recorded during the 1968 Tokachi-Oki Earthquake and the JMA-Kobe motions recorded during the 1995 Hyogoken-Nanbu Earthquake, which are oceanic type and epicentral type earthquakes, respectively, have the same Fourier amplitude; in other words, the same total energy input at the vicinity of 1·0-s period, but they exhibit a considerable difference in destructiveness to structures of 1·0-s natural period in such a way that the epicentral motions having a larger rate of energy input in the time domain can knock down the structures more devastatingly than the oceanic type motions.[9,10] From the fact that time-sequential characteristics of energy input as well as total accumulation of energy input has a significant effect on structural safety, it is now recognized that a method to analyse and simulate earthquake motions in both time and frequency domains is needed for structural safety estimation.

Recently, wavelet analysis is getting utilized as a method of transforming time-sequential data to data on a time–frequency plane, especially in the field of signal processing in electrical and electronics engineering,[11] but is not yet applied to seismic engineering from the viewpoint of dynamic responses of structures. One of the most attractiveness in wavelet transform, which is unavailable in Fourier transform, is that the wavelet coefficients deduced from time-sequential acceleration data represent the components of energy input in time and frequency domains.[12] In this paper, first, the fundamentals of wavelet analysis are introduced in view of energy input towards the application to earthquake engineering in conjunction with the conventional Fourier analysis. On the basis of energy theorem in wavelet analysis, which is developed in this study, the wavelet transform is applied to the acceleration records of the 1995 Hyogoken-Nanbu Earthquake to identify the time–frequency characteristics of epicentral earthquake motions. As a final goal, a method is proposed for computationally simulating earthquake accelerations whose properties are controlled in time domain as well as in frequency domain by means of wavelet inverse transform.

2. RELATIONS BETWEEN WAVELET, FOURIER, AND ENERGY

2.1. Fundamentals of wavelet transform

Since details of wavelet transform are lectured in some textbooks,[13] the basic principles which are necessary to apply wavelet transform to earthquake motion analysis are summarized herein. There are two types of wavelet transforms, that is, the continuous wavelet transform and the discrete wavelet transform, both of which are utilized to expand time-sequential data onto a time-frequency plane. From a practical viewpoint of data analysis, the discrete wavelet transform is more useful because transformed data by the discrete wavelet transform have no redundant components and then the inverse transform can be applied to any family of time-frequency data. Therefore, in this paper, discrete wavelet transform will be used and be called simply wavelet transform.

Wavelet transform decomposes $f_i(t)$, a function of time t, to lower level functions as follows:

$$f_i(t) = f_{i-1}(t) + g_{i-1}(t) \tag{1}$$

Therefore, the original function $f_i(t)$ can be expanded to a series of level functions $g_j(t)$'s as follows:

$$f_i(t) = \sum_{j=-\infty}^{i-1} g_j(t) \tag{2}$$

where $g_j(t)$ can be expressed by a linear combination of wavelet functions as follows:

$$g_j(t) = \sum_{k=-\infty}^{\infty} \alpha_{j,k} \cdot \psi_{j,k} \tag{3}$$

$$\psi_{j,k} = 2^{j/2}\psi\ (2^j t - k) \tag{4}$$

where j and k are integers called frequency level (or simply, level) and time index, respectively, $\alpha_{j,k}$ is called the wavelet coefficient, and ψ is called the wavelet function. Many mathematical forms for wavelet function ψ which enable the linear combination of equation (3) have been developed by Daubechies,[14] Chui,[15] Meyer[16] and many other researchers, but in this study the wavelet function of 10-th order Daubechies shown in Figure 1 is used due to its orthogonality and satisfactory resolution in both time and frequency.

Since ψ has non-zero values only in a limited range in the time domain as well as in the frequency domain, $g_j(t)$ defined as a sum of these wavelet functions by equation (3) has energy only in a particular range of frequency. The level designated by j is an index representing the frequency range such that a smaller j corresponds to a range of lower frequencies, and then $g_j(t)$ for a lower j has components of lower frequencies. While k is an index denoting the predominant time at which the wavelet function ψ appears as shown in Figure 2 which illustrates two components for k and $k + 1$ in the series of equation 3. When ψ has a peak value at t_c in the local time for defining the ψ as shown in Figure 1, the peak of $k -$ component of $g_j(t)$ in equation (3) appears at $t_{j,k}$ given by the following equation which is derived from equating the term in the parenthesis of ψ in equation (3) with t_c:

$$t_{j,k} = 2^{-j}(t_c + k) \tag{5}$$

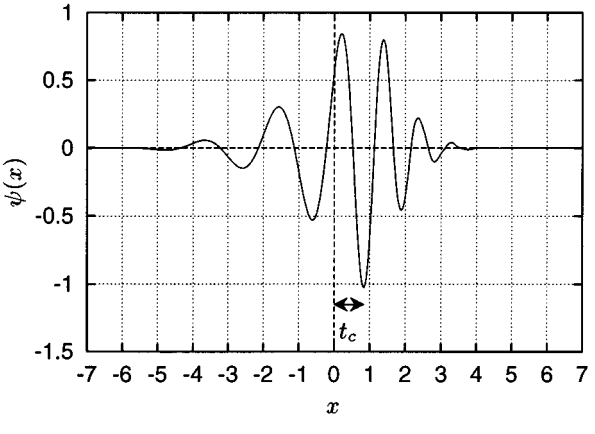

Figure 1. Example of wavelet function (Daubechies $N = 10$)

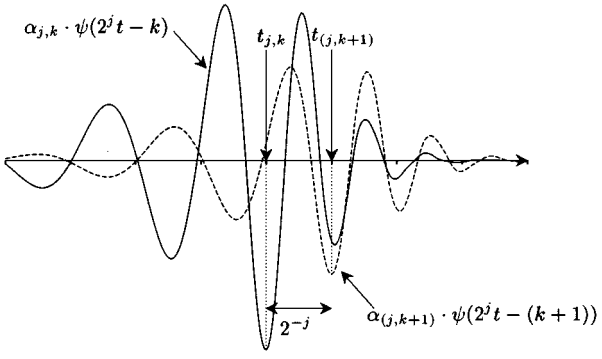

Figure 2. k and $k+1$ components of $g_j(t)$

The time $t_{j,k}$ is called the representative time for level j and time index k. Since k is an integer, $t_{j,k}$ is a time point which locates discretely at a longer interval for a smaller j. The above information implies that the wavelet coefficient $\alpha_{j,k}$ represents a signal intensity of level j at the vicinity of $t_{j,k}$.

In practice, the original time-sequential function is set to be a level 0 function denoted by $f_0(t)$, which requires that the time interval of the digital data constituting $f_0(t)$ must be 1 on the condition that the data in the original function are in one-to-one correspondence with the series of wavelet coefficients. However, since the time interval Δt of earthquake acceleration data is not necessarily equal to 1, the times allotted to wavelet coefficients are all multiplied by Δt in the following calculation process.

As an example, results of wavelet transform applied to the 1940 El Centro NS acceleration data are shown in Figure 3. The graphs an the left-hand side show the acceleration waves of original and four-level functions, i.e. f_0 and $g_j(t)$ for $j = -3, -4, -5,$ and -6. The graphs on the right-hand side show the wavelet coefficients $\alpha_{j,k}$ of the corresponding levels at time points designated by $t_{j,k}$, in which the height of a bar represents the value of $\alpha_{j,k}$. It is observed that the envelope curve of $\alpha_{j,k}$ is similar to that of $g_j(t)$, which suggests that wavelet coefficient $\alpha_{j,k}$ represents the accelerational intensity of frequency level j at time $t_{j,k}$.

2.2. *Energy principles in wavelet analysis*

One of the great benefits of applying wavelet transform to earthquake motion analyses lies in energy principles developed in this study, from which energy components hidden in motions can be disclosed in time and frequency domains simultaneously. Since it is known that time history of energy input during an earthquake is similar to that of acceleration power of ground motions,[5] the relations between wavelet and acceleration power are first investigated. Acceleration power I_E of the original acceleration wave $f_0(t)$ is expressed from its definition and is rewritten from equation (2) as follows:

$$I_E \equiv \int_{-\infty}^{\infty} f_0(t)^2 \, \mathrm{d}t = \sum_{j=-\infty}^{-1} \int_{-\infty}^{\infty} g_j(t)^2 \, \mathrm{d}t + \sum_{m \neq n} \int_{-\infty}^{\infty} g_m(t) \cdot g_n(t) \, \mathrm{d}t \tag{6}$$

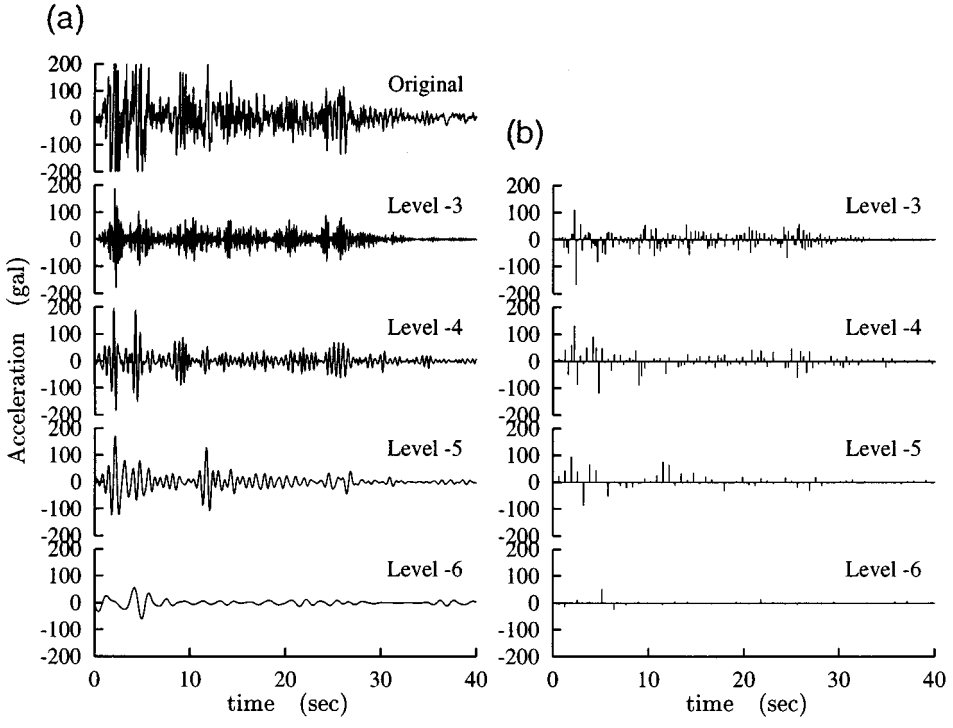

Figure 3. $g_j(t)$ and $\alpha_{j,k}$ of the 1940 El Centro NS accelerations: (a) $g_j(t)$; (b) $\alpha_{j,k}$

When ψ constituting $g_j(t)$ of equation (3) is a semi-orthogonal or an orthogonal wavelet, the second term on the right-hand side of equation (6) vanishes. Therefore,

$$I_{\mathrm{E}} = \sum_{j=-\infty}^{-1} \int_{-\infty}^{\infty} g_j(t)^2 \, \mathrm{d}t \tag{7}$$

This equation means the I_E of $f_0(t)$ can be decomposed into acceleration power of each level as follows:

$$I_E = \sum_{j=-\infty}^{-1} I_{E_j} \tag{8}$$

$$I_{E_j} = \int_{-\infty}^{\infty} g_j(t)^2 \, \mathrm{d}t \tag{9}$$

The acceleration power of each level, I_{E_j}, is related to the Fourier amplitude through the following equation by Parseval's identity:

$$I_{E_j} = 2 \int_0^{\infty} |F_j(v)|^2 \, \mathrm{d}v \tag{10}$$

where $|F_j(v)|$ is the Fourier amplitude at frequency v of the level function $g_j(t)$.

Since, as mentioned before, each level function $g_j(t)$ has a range of particular frequencies out of which the intensity is zero, a supposition is introduced here that the original function $f_0(t)$ is decomposed into a series of $g_j(t)$'s exclusively in the frequency domain; in other words, each $g_j(t)$ has non-zero components only in an exclusive range of frequency. This supposition is not theoretically exact but is justified later from a viewpoint of engineering practice. The exclusive range of frequency of $g_j(t)$ is denoted as follows:

$$\text{frequency range of level } j = [\nu_{1j}, \nu_{2j}] \tag{11}$$

or

$$\text{period range of level } j = [T_{1j}, T_{2j}] \tag{12}$$

From the nature of discrete wavelet transform that $g_j(t)$ has components of half frequency of $g_{j+1}(t)$[13], ν_{1j}, ν_{2j}, T_{1j}, and T_{2j} are expressed as follows:

$$\nu_{1j} = 2^{j-1}/\Delta t, \qquad \nu_{2j} = 2^j/\Delta t \tag{13}$$

$$T_{1j} = 2^{-j}\Delta t, \qquad T_{2j} = 2^{-j+1}\Delta t \tag{14}$$

where Δt is the time step of digital data of $f_0(t)$.

Under this supposition, equation (10) can be rewritten by the following integration :

$$I_{E_j} = 2\int_{\nu_{1j}}^{\nu_{2j}} |F(\nu)|^2 \, \mathrm{d}\nu \tag{15}$$

where $|F(\nu)|$ is the Fourier amplitude of the original function $f_0(t)$.

Figure 4 shows the Fourier amplitude spectra of $f_0(t)$ and $g_j(t)$ shown in Figure 3a. The dotted line in each graph is the spectrum of the original $f_0(t)$. It is observed that each $g_j(t)$ occupies a range of particular frequencies of the Fourier amplitude spectrum of the original $f_0(t)$ in such a way that $g_j(t)$ of a smaller j covers the range of lower frequencies, i.e. longer periods. Unfortunately, however, there is an overlap in frequency between adjacent levels. It is known that the width of the overlap depends on used wavelet function ψ. The Daubechies wavelet function of a high order which is used in this study gives a relatively small overlap, which means that it has a good resolution in the frequency domain, while it has a relatively long range in time as shown in Figure 1, which means it has a poor resolution in time domain. Therefore, the wavelet should be chosen appropriately on the consideration of the requested precision in favour of frequency or time because of unavoidable trade-off between them. In this paper, every $g_j(t)$ is assumed to have an exclusive frequency range of equation (11), disregarding the overlap. This assumption means the total energy of the original wave is divided to $g_j(t)$'s exclusively.

When the wavelet function ψ is orthogonal, $\alpha_{j,k}$ as well as I_{E_j} has more effective relationships with the Fourier amplitude spectrum in the following discussion. Here, energy input E_j of level j is defined as an average of the square of Fourier amplitude in the frequency range of level j as follows:

$$E_j = \frac{1}{\nu_{2j} - \nu_{1j}} \int_{\nu_{1j}}^{\nu_{2j}} |F(\nu)|^2 \, \mathrm{d}\nu \tag{16}$$

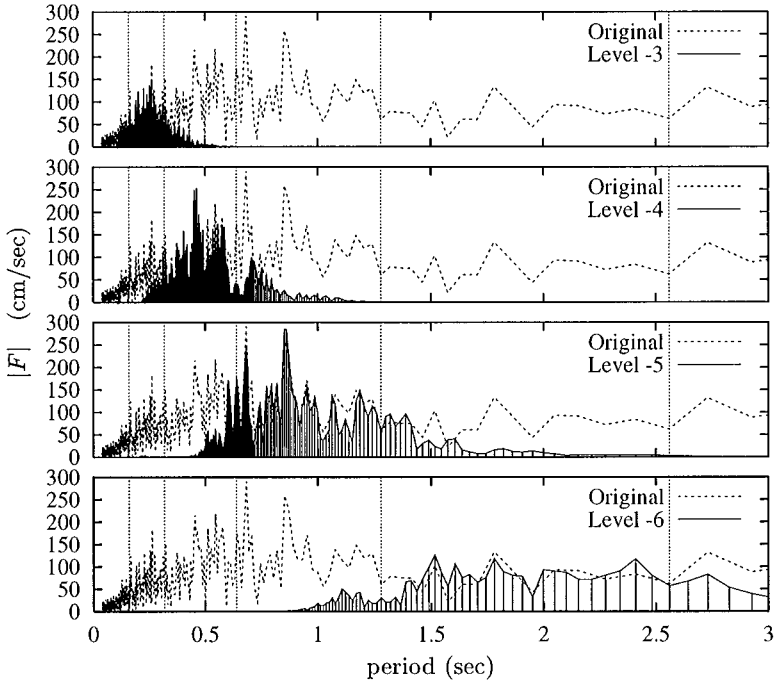

Figure 4. Fourier amplitude spectra of $f_0(t)$ and $g_j(t)$ of the 1940 El Centro NS accelerations

The acceleration power I_{E_j} of equation (9) is expressed as follows from equation (3) due to the orthogonality of ψ with a new variable $x = 2^j t - k$:

$$I_{E_j} = \Delta t \sum_{k=-\infty}^{\infty} \alpha_{j,k}{}^2 \int_{-\infty}^{\infty} \{\psi(x)\}^2 \, \mathrm{d}x = \Delta t \sum_{k=-\infty}^{\infty} \alpha_{j,k}{}^2 \tag{17}$$

because

$$\int_{-\infty}^{\infty} \{\psi(x)\}^2 \, \mathrm{d}x = 1 \tag{18}$$

in case that $\psi(x)$ is an orthonormal wavelet. By substituting equations (13)–(15) and (17) into equation (16), E_j is expressed as follows:

$$E_j = 2^{-j} \Delta t^2 \sum_{k=-\infty}^{\infty} \alpha_{j,k}{}^2 \tag{19}$$

Since as given by equation (16), E_j has a dimension of square of Fourier amplitude of ground accelerations and is averaged in the frequency range of level j of equation (11), E_j is equal to the average energy input into an SDOF system having a mass of 2 with a period belonging to the period range of level j of equation (12). Thus, E_j is simply called energy input of level j in the following discussion.

Considering the parameter k is an index for the time where $\alpha_{j,k}$ gives the peak intensity of energy of level j, k-component in E_j of equation (19), which is called the instantaneous energy input and is denoted by $\Delta E_{j,k}$ as follows, represents the energy input at the vicinity of time $t_{j,k}\Delta t$ during a time span of $2^{-j}\Delta t$ which is calculated from $(t_{(j,k+1)} - t_{j,k})\Delta t$ by using equation (5):

$$\Delta E_{j,k} = 2^{-j}\Delta t^2 {\alpha_{j,k}}^2 \tag{20}$$

The sum of $\Delta E_{j,k}$ up to k, which is denoted by $E_{j,k}$ as follows, is the cummulative energy input of level j until time $t_{j,k}\Delta t$:

$$E_{j,k} = 2^{-j}\Delta t^2 \sum_{l=-\infty}^{k} \alpha_{(j,l)}^2 \tag{21}$$

The above equations (19)–(21) are called energy principles in wavelet analysis. In a strict sense, however, $\Delta E_{j,k}$ and $E_{j,k}$ are not equal to the time history of energy input to a structure, because the time history of energy input is affected even by dynamic properties of the structure.[9] However, noticing that the time duration $2^{-j}\Delta t$ between the adjacent wavelet coefficients is equal to half the T_{2j} of equation (14), $\Delta E_{j,k}$ and $E_{j,k}$ are considered important hazardous properties of earthquake motions, because the rate of energy input defined as energy input during a half of structure's natural period causes the maximum displacement response and then gives a significant effect on structural safety.[9,10]

3. WAVELET CHARACTERISTICS OF THE 1995 HYOGOKEN-NANBU EARTHQUAKE MOTIONS

3.1. Used acceleration records

Applying the energy principles of wavelet analysis developed in the above discussion to the 1995 Hyogoken-Nanbu Earthquake motions, the time histories of energy input in different frequency levels are investigated herein. Typical tendencies of energy input on a time–frequency plane of epicentral earthquake motions will be identified.

The earthquake ground accelerations recorded at 33 sites during the earthquake are used, which were published by the Architectural Institute of Japan.[17] Figure 5 shows the map in which the observation sites around Kobe and Osaka are plotted.

3.2. Time-frequency characteristics of energy input

Typical time histories of energy input in four frequency levels of the earthquake motions recorded at three different sites are shown in Figure 6, in which cases (1), (2), and (3) correspond to the sites close to, moderately far from, and very far from the epicentre, respectively. In each figure, the upper graph shows the time history of acceleration record and the lower one the time history of energy input $E_{j,k}$, in which four lines denote different frequency levels whose ranges are defined by equations (11) or (12). It is observed from Figure 6(1) for a site near the epicentre that all the frequency components appear almost at the same time followed by a sharp increase of energy input per second. In contrast, at sites far from the epicentre of Figure 6(2) longer period components appear later after the shorter period components. The gradients of the time history

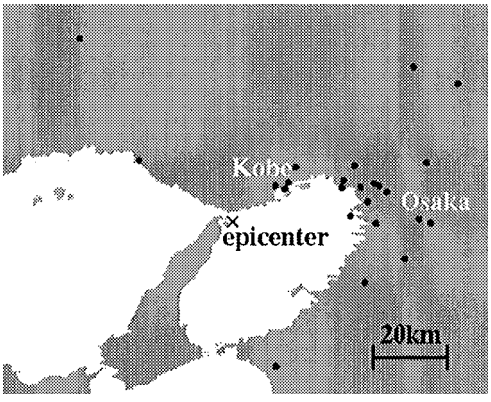

Figure 5. Observation sites of the 1995 Hyogoken-Nanbu Earthquake

curves, that is called 'input rate', is proportional to the total amount of energy input, irrespective of the frequency and the epicentral distance.

3.3. Total energy input

Figure 7 shows the relations between E_j of equations (19) and the epicentral distance. E_j is the total energy input for level j accumulated until the end of the earthquake motions. It is found that E_j for each level decreases rapidly with the epicentral distance, noticing that E_j is logarithmically presented in the figure, but keeps a stable value for a distance greater than 100 km. The order of E_j's for five frequency levels is kept basically consistent over the entire range of distance from 15 to 200 km. Thus, there is no apparent evidence in this earthquake to support the idea that the motions at a farther distance from the epicentre possess a large amplitude at a longer period.

3.4. Rate of energy input

Figure 8 shows the relationship between $\Delta E_{j\max}$ and the epicentral distance. $\Delta E_{j\max}$, which is named maximum instantaneous energy input, is the maximum of $\Delta E_{j,k}$ of equation (20) with respect to k defined as

$$\Delta E_{j\max} = \max_k \{\Delta E_{j,k}\} \tag{22}$$

With the increase of epicentral distance, $\Delta E_{j\max}$ decreases up to the distance of 100 km. The basic feature is similar to the total energy input of Figure 7. The relation between the total and the maximum instantaneous energy inputs is shown in Figure 9, from which it is found that there is a strong positive correlation between the total and the maximum instantaneous energy inputs.

Figure 10 shows the ratio of the maximum instantaneous energy input to the total energy input. The plotted data marked by $\times$ are placed at five locations in the axis of natural period, which correspond to the centre periods of period ranges of five levels. The dotted lines and error bars in the figure denote the averages and the standard deviations of 33 data, respectively. There

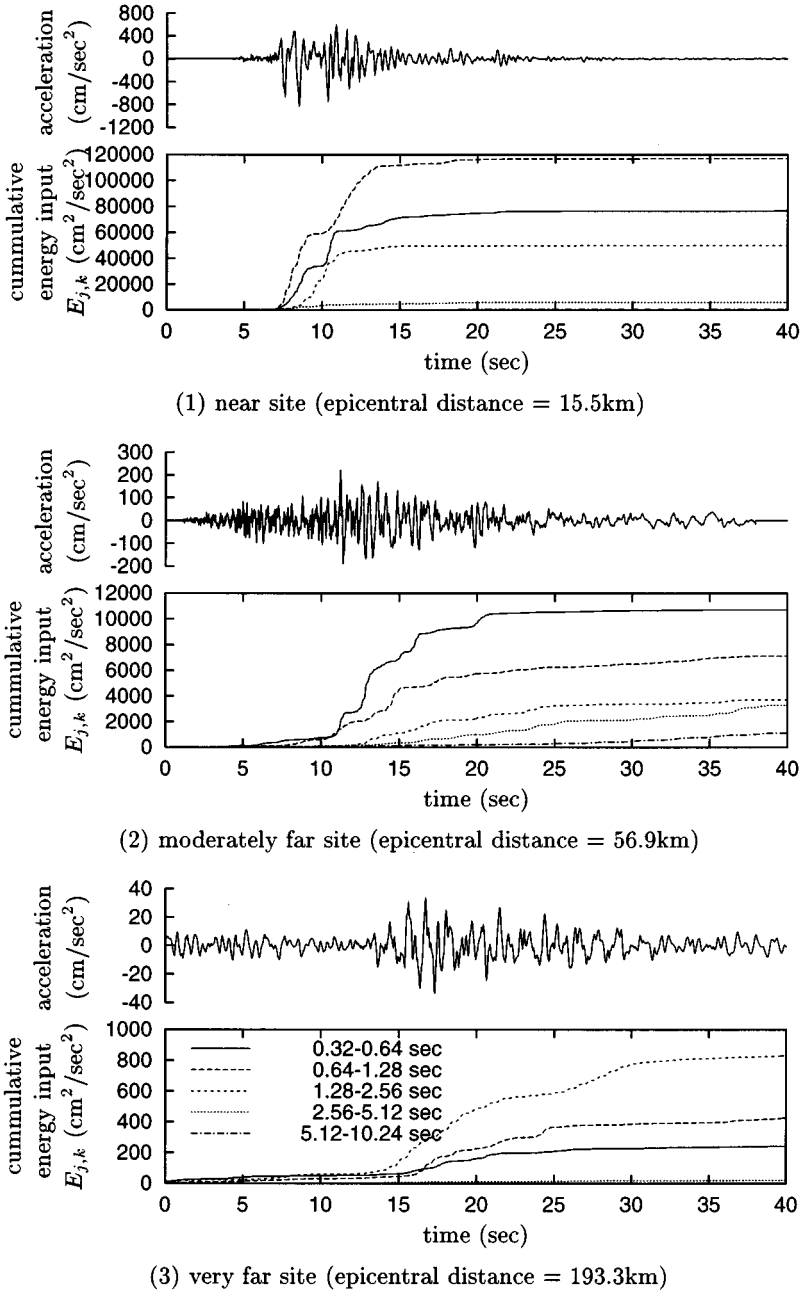

Figure 6. Accumulation patterns of energy input in time and frequency domains for three sites of different epicentral distances during the 1995 Hyogoken-Nanbu Earthquake

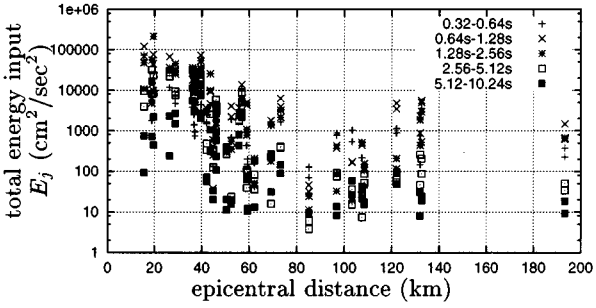

Figure 7. Total energy input vs. epicentral distance of the 1995 Hyogoken-Nanbu Earthquake motions

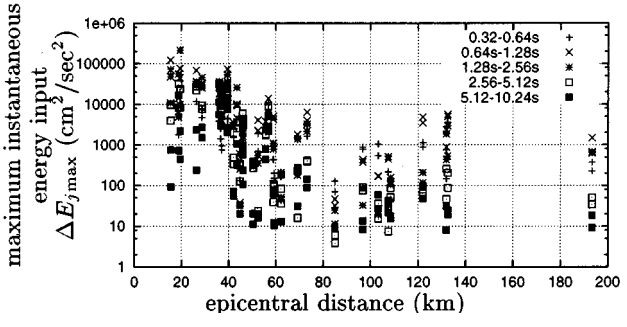

Figure. 8. Maximum instantaneous energy input vs. epicentral distance of the 1995 Hyogoken-Nanbu Earthquake motions

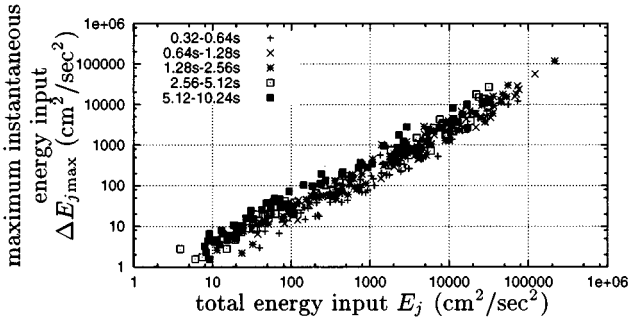

Figure 9. Maximum instantaneous energy input vs. total energy input of the 1995 Hyogoken-Nanbu Earthquake motions

is a tendency that components of lower levels or longer periods have larger ratios of instantaneous energy input to total input.

Next, the average rate of energy input during an effective duration is investigated, which is defined as follows:

$$\overline{\Delta E_j} = \frac{0.8E_j}{\Delta t_{je}} \tag{23}$$

$$\Delta t_{je} = t_{j90} - t_{j10} \text{ for level } j \text{ input} \tag{24}$$

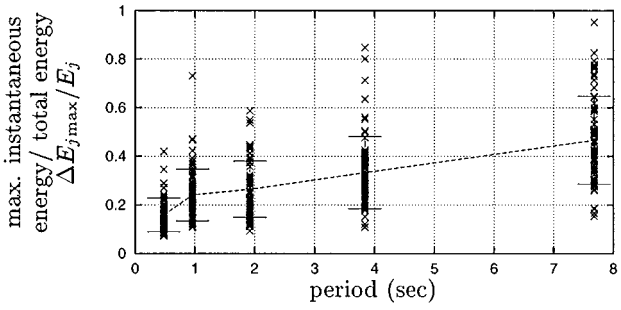

Figure 10. Ratio of maximum instantaneous energy input to total energy input of the 1995 Hyogoken-Nanbu Earthquake motions

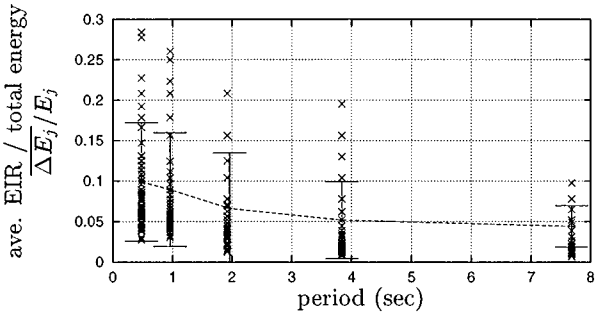

Figure 11. Ratio of average energy input rate to total energy input of the 1995 Hyogoken-Nanbu Earthquake motions

where

$$t_{j10} = \text{time when } E_{j,k} \text{ reaches 10\% of } E_j \tag{25}$$

$$t_{j90} = \text{time when } E_{j,k} \text{ reaches 90\% of } E_j \tag{26}$$

Figure 11 shows the relation between the effective duration and frequency level 1 by noticing $\overline{\Delta E_j}/E_j = 0.8/\Delta t_{je}$. It is observed that motions of a lower level, i.e. a longer period need a longer duration to accumulate 80 percent of the energy of the level.

3.5. Predominant time of energy input

In Figure 12, the relation between predominant time $t_{j\text{pred}}$ and epicentral distance is shown. The predominant time $t_{j\text{pred}}$ is defined as

$$t_{j\text{pred}} = t_{(j,k_1)} \cdot \Delta t - t_{10} \tag{27}$$

in which k_1 is the time index where the instantaneous energy input $\Delta E_{j,k}$ takes the maximum value among all possible k's for j and t_{10} is the time when 10 percent of I_E of equation (6) is fulfilled. It is noted from Figure 12 that maximum instantaneous energy input appears quickly

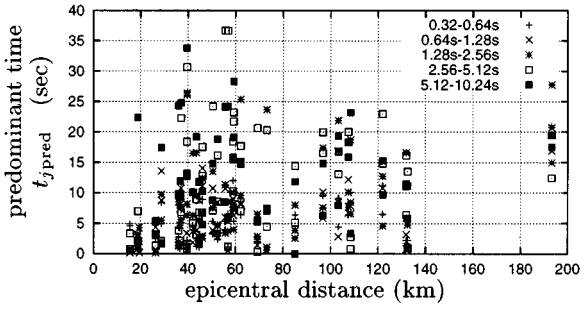

Figure 12. $t_{j\text{pred}}$ vs. epicentral distance of the 1995 Hyogoken-Nanbu Earthquake motions

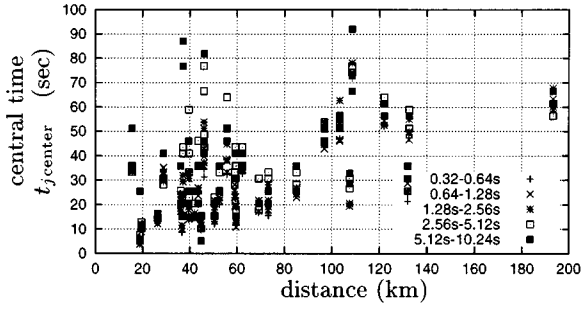

Figure 13. $t_{j\text{centre}}$ vs. epicentral distance of the 1995 Hyogoken-Nanbu Earthquake motions

after the beginning of the earthquake for all frequency levels in the epicentral region within a 20 km radius. However, with the increase of epicentral distance, $t_{j\text{pred}}$ tends to increase and the maximum instantaneous energy inputs of longer-period components tend to appear later than shorter-period components.

Figure 13 shows the relation between central time $t_{j\text{centre}}$ and epicentral distance. The central time $t_{j\text{centre}}$ is defined as

$$t_{j\text{centre}} = t_{j50} - t_{10} \tag{28}$$

in which t_{j50} is the time when $E_{j,k}$ reaches half of E_j. It is observed that $t_{j\text{centre}}$ has the same tendency as $t_{j\text{pred}}$ in a more apparent way that longer-period components appear later than shorter-period components.

4. METHOD OF SIMULATING EARTHQUAKE MOTIONS CONTROLLED IN BOTH TIME AND FREQUENCY DOMAINS

4.1. Target time–frequency characteristics

As discussed in the previous sections, earthquake ground acceleration data are transformed into time series of wavelet coefficients for different frequency levels from which valuable information that

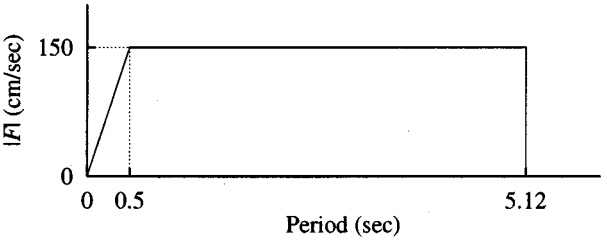

Figure 14. Target Fourier amplitude spectrum

might govern structural dynamic behaviours can be withdrawn. In these sections, three properties of earthquake ground motions, i.e. Fourier amplitude, predominant time, and rate of energy input, are focused and are selected as control parameters to make computer-simulated earthquake accelerations by means of wavelet inverse transform.

The first controlled property is the Fourier amplitude spectrum, because the total energy input during an earthquake is governed by the Fourier amplitude. The shape of the Fourier amplitude spectrum is assumed bilinear, as shown in Figure 14 merely for the sake of simplicity. In this study, Δt is 0.01 s and eight levels from -1 to -8 are considered. This means the Fourier amplitude spectrum has energy only in a period range from 0·02 to 5·12 s as derived from equation (14), which covers most of natural periods of low-rise to high-rise building structures. The second property is the predominant time of energy input. In this study, the predominant times of lower levels appear later than those of higher levels as shown in Figure 15 with a linear relationship between $t_{j\text{pred}}$ and $(T_{1j} + T_{2j})/2$. The third property is the rate of energy input, which is defined by the time history curve of energy input in Figure 16. The time history curve is assumed a cubic equation in this study and the duration of energy input is assumed 5 s, from which the instantaneous energy input $\Delta E_{j,k}$ and average energy input rate $\overline{\Delta E_j}$ mentioned in Section 3.4 are automatically determined.

4.2. *Method of simulating earthquake accelerations*

The essence of the method of simulating earthquake ground motions is to make $\alpha_{j,k}$ series, from which the simulated accelerograms can be acquired by the inverse wavelet transform. The $\alpha_{j,k}$ sequence is generated to meet the three target characteristics defined in the previous section.

First, the total energy of each level must be equal to the energy calculated from the Fourier amplitude spectrum. This condition is expressed as follows from equations (16) and (19):

$$\sum_{k=-\infty}^{\infty} {\alpha_{j,k}}^2 = \frac{2^j}{\Delta t^2 (v_{2j} - v_{1j})} \int_{v_{1j}}^{v_{2j}} |F(v)|^2 \, \mathrm{d}v \tag{29}$$

in which $|F(v)|$ must meet the target spectrum of Figure 14.

The second condition is that the predominant time $t_{j\text{pred}}$ for each level defined by equation (27) must agree with the target shown in Figure 15, which is expressed as follows:

$$t_{j\text{pred}} = \frac{15}{5.1} \left(\frac{T_{1j} + T_{2j}}{2} - 0.02 \right) + 5 \tag{30}$$

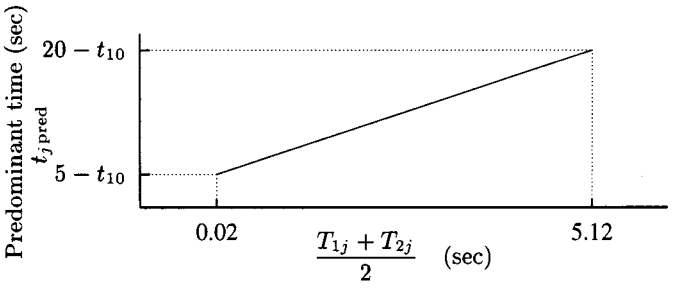

Figure 15. Target predominant time

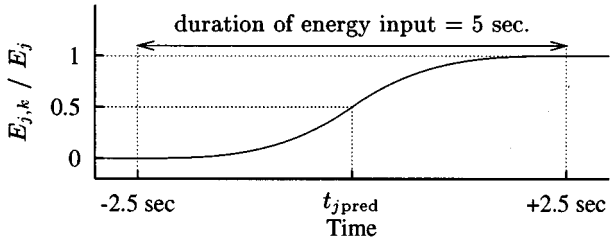

Figure 16. Target time history of energy input

The third condition is that the time history of energy input of each level $E_{j,k}$ must be in accordance with the cubic curve of Figure 16. This is satisfied by making the amplitude of $\alpha_{j,k}$ series in the time domain trace the linear envelope functions given by dotted lines in Figure 17, because an integration of square of a linear function, which is proceeded by equation (21), becomes a cubic function. Considering the fact that the values of $\alpha_{j,k}$ series vibrate in the envelope curve as demonstrated in Figure 3, uniform random numbers between -1 and $+1$ are adopted in order to vibrate $\alpha_{j,k}$. Consequently, products of the uniform random numbers and the linear envelope function are assigned to the values of $\alpha_{j,k}$ series for generating waves. An example of $\alpha_{j,k}$ series is shown as bars in Figure 17.

After making $\alpha_{j,k}$ series which satisfy the three target properties, it is easy to make the time-sequential acceleration data by inverse wavelet transform. An example of generated earthquake accelerations is shown in Figure 18. The accelerogram of Figure 18 may not really look like an actual accelerogram such as early decay of high-frequency components. But this defect is permitted at the present state for establishing a basic method of generating accelerograms having target time–frequency characteristics.

4.3. Energy input of the simulated waves

4.3.1. Energy-based velocity spectrum. In Figure 19, energy-based velocity spectra $V_E(T)$ defined by equation (31) induced by five simulated accelerograms are shown:

$$V_E(T) = \sqrt{\frac{2E(T)}{M}} \tag{31}$$

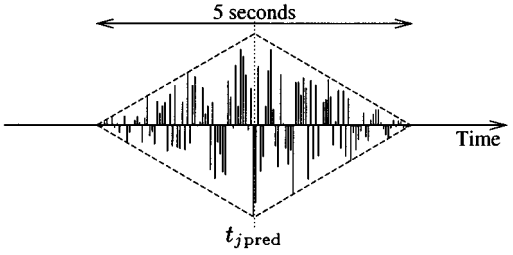

Figure 17. Linear envelope function and generated $\alpha_{j,k}$ series therein

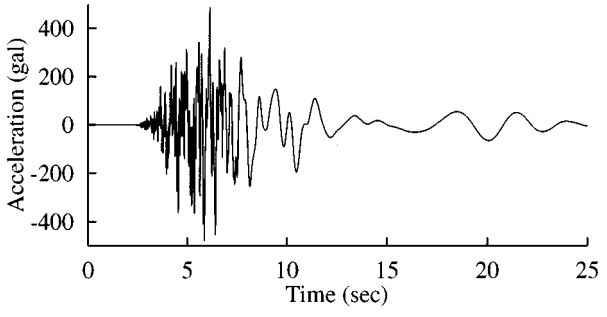

Figure 18. An example of simulated earthquake accelerations complying with the target time–frequency properties specified by Figures 14–16

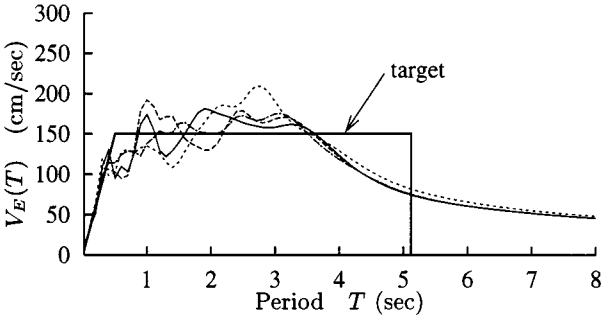

Figure 19. Energy-based velocity spectra of five simulated accelerations

where $E(T)$ is the total energy input to a 10 percent-damped SDOF system with natural period T, and M is the mass. The five simulated accelerograms are generated by the method of Section 4.2 using five different sets of random numbers.

The average of the five spectra seems to converge to the target spectrum, but their fluctuating range is so wide that the precision of controlling the total energy input is not high. This is because the proposed method can give only one value to the Fourier amplitude spectrum covering

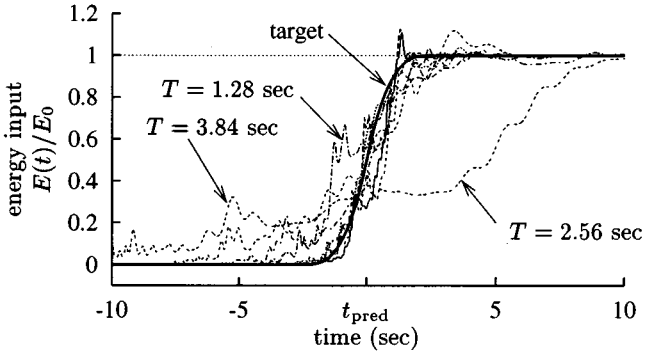

Figure 20. Time histories of energy input of simulated motions

a relatively wide frequency range, which is a defect inherent to wavelet inverse transform. But some advanced attempts are going to be made to improve such poor resolution in wavelet inverse transform, in which the Fourier phase spectrum is modified according to wavelet characteristics.[12]

4.3.2. Predominant time and time history of energy input. In Figure 20 time histories of energy input of the five simulated motions to 10 percent-damped linear SDOF systems having natural periods, 0·32, 0·48, 0·96, 1·28, 1·92, 2·56, and 3·84 seconds are shown. The energy input $E(t)$ until time t is normalized by the total energy input E_0 at the end of motions. The periods are selected from T_{1j}, T_{2j}, and $(T_{1j} + T_{2j})/2$ of $j = -4, -5, -6$ and -7. In the figure, the predominant time t_{pred} of the SDOF system, which is acquired from Figure 15 regarding the x-axis of the figure as the natural period of the system, of each curve is adjusted to 0 in time axis. The thick line shows the target curve. All the lines in the figure are almost similar to the target curve, which means the proposed method can properly control the predominant time and time history of energy input. However, the curves for longer natural periods are not satisfactorily close to the target curve, because wavelet coefficients for lower levels are distributed sparsely in the duration of motions.

5. CONCLUSIONS

In this paper, a method of applying wavelet transform to earthquake motion analysis is developed from the viewpoint of energy input to structures. Wavelet transform is a mathematical tool which transforms sequential data in time axis such as earthquake accelerations to spectral data in both time and frequency. Therefore, wavelet transform provides information on non-stationary time-dependent intensity of motions regarding a particular frequency of interest.

First, an energy theorem is developed, which states that the square of an individual wavelet coefficient deduced from acceleration data by the wavelet transform is proportional to the instantaneous energy input introduced in a range of time and frequency assigned to the wavelet coefficient.

Second, the 1995 Hyogoken-Nanbu earthquake ground motions were wavelet transformed into spectral components in time and frequency domains. On the basis of the energy theorem, the

following tendencies were observed: waves of shorter and longer periods discharge energy at the same time in the epicentral region, while with the increase of epicentral distance waves of longer periods appear later than waves of shorter periods; maximum instantaneous energy input is proportional to the total energy input irrespective of frequency; and the ratio of the maximum instantaneous energy input to the total energy input is larger for waves of longer periods.

Third, a method of making computer-simulated earthquake accelerations was developed by means of the wavelet inverse transform, in which the accelerations were simulated according to a given history of instantaneous energy input specified for each frequency component. It was shown that structural responses of 10 percent-damped linear SDOF systems to the simulated accelerations have a satisfactory agreement with the target energy spectrum and target history of energy input. This result strongly supports that the wavelet coefficients represent energy responses of structures.

At the present time, wavelet transform has scarcely been applied to earthquake engineering. However, it seems a powerful analytical tool to identify the input motion characteristics in both time and frequency which governs the dynamic behaviours of structures and their safety. Therefore, further study is expected to utilize wavelet transform techniques in earthquake engineering, and the problem associated with sparseness of wavelet coefficient distribution and the method of selecting an optimum shape of mother wavelets should be investigated.

REFERENCES

1. G.W. Housner, 'Behavior of structures during earthquakes, *J. Engng Mech. Div. Proc. American Society of Civil Engineers*, *ASCE*, **85**(EM 4), 109–129 (1959).
2. A. S. Veletsos and N. M. Newmark, Effect of inelastic behavior on the response of simple systems to earthquake motions, *Proc. 2nd WCEE*, Vol. 2, Japan, 1960, pp. 895–912.
3. G. V. Berg and S. S. Thomaides, 'Energy consumption by structures in strong-motion earthquakes', Proc. 2nd WCEE, Japan, Vol. 2, 1960, pp. 681–697.
4. B. Kato and H. Akiyama, 'Seismic design of steel buildings, the Journal of the Structural Division', *Proc Amer. Soci. Civil Engng*, *ASCE*, **108**(ST8), 1709–1721, (1982).
5. H. Kuwamura and T. V. Galambos, 'Earthquake load for structural reliability,' *J. Struct. Engng*, *ASCE*, **115**(6), 1446–1462, (1989).
6. C. Uang and V. V. Bertero, 'Evaluation of seismic energy in structures', *Earthquake Engng. Struct. Dyn.* **19,** 77–90 (1990).
7. P. Fajfar and T. Vidic, 'Consistent inelastic design spectra: hysteric and input energy', *Earthquake Engng Struct. Dyn.* **23,** 523-537 (1994).
8. H. Kuwamura, Y. Kirino and H. Akiyama, 'Prediction of earthquake energy input from smoothed Fourier amplitude spectrum', *Earthquake Engng. Struct. Dyn.* **23,** 1125–1137 (1994).
9. H. Kuwamura, T. Takeda, and Y Sato, 'Energy input rate in earthquake destructiveness — Comparison between epicentral and oceanic earthquakes', *J. Struct. Constr. Engng.* (491), 29–36, (1997). (in Japanese).
10. H. Kuwamura, J. Iyama and T. Takeda, 'Energy input rate of earthquake ground motion — matching of displacement theory and energy theory', *J. Struct. Constr. Engng.* (498), 37–42, (1997). (in Japanese).
11. .M. Combes, A. Grossmann and Ph. Tchamitchian (eds), *Wavelets: Time-Frequency Methods and Phase Space*, *Proc. Int. Conf.* Marseille, France, 14–18 December 1987, Springer, Berlin, 1989.
12. J. Iyama and H. Kuwamura, 'Application of wavelet inverse transformation for numerically simulated earthquake motions', *J. Struct. Constr. Engng.* (502), 47–52, (1997) (in Japanese).
13. J. J. Benedetto and M. W. Frazier, *WAVELETS: Mathematics and Applications*, CRC Press, Boca Raton, FL, 1994.
14. I. Daubechies, 'Orthonormal bases of compactly supported wavelets', *Commun. Pure Appl. Math.* **41,** 909–996 (1988).
15. C.K. Chui and J.Z. Wang, 'On compactly supported spline wavelets and a duality principle', *Trans. Amer. Math. Soc.* **330** 903–915 (1992).
16. Y. Meyer, 'Orthonormal Wavelets', in *Wavelets, Proc. Int. Conf.* France, Springer, Berlin, 1989.
17. Architectural Institute of Japan, *Report on Acceleration Records of the* 1995 *Hyogoken-Nanbu Earthquake*, 1996 (in Japanese).

